ELSEVIER

Applied Acoustics 64 (2003) 287–310

applied acoustics

www.elsevier.com/locate/apacoust

Assessing the effect of a barrier between two rooms subjected to low frequency sound using the boundary element method

A. Tadeu*, P. Santos

University of Coimbra, Department of Civil Engineering, 3030-290 Coimbra, Portugal

Received 23 November 2001; received in revised form 5 August 2002; accepted 9 August 2002

Abstract

The boundary element method (BEM) has been used to compute the acoustic wave propagation through a single vertical panel, which separates two rooms, made of concrete, when one of the rooms is excited by a steady-state, spatially sinusoidal, harmonic line load pressure at low frequencies. This work focuses on how the connection of the panel to the ceiling affects the acoustic insulation provided by the wall. Perfect double-fixed partitions and acoustic barrier-type structures with differently-sized gaps between the ceiling and the barrier are studied. The BEM model is formulated in the frequency domain and takes the air-solid interaction fully into account. Insulation dips are localised in the frequency domain and identified with dips associated with both the wall's natural dynamic vibration modes and with those associated with the air in the rooms. The influence of the wall's thickness on acoustic insulation is also analysed. The computed results obtained with the acoustic barrier type structure are compared with those obtained by a rigid model. The importance of the rooms' surface conditions is assessed, modelling the rooms with cork.

Keywords: Acoustic insulation; Boundary elements method; Acoustic barrier

1. Introduction

Besides the mass and sound frequency, there are other variables that may affect the acoustic insulation of a separation element. Among these are the angle of

* Corresponding author. Tel.: +351-239797201; fax: +351-239797190.
E-mail address: tadeu@dec.uc.pt (A. Tadeu).

0003-682X/02/$ - see front matter
PII: S0003-682X(02)00074-9

incidence of the incident sound waves, the presence of weaker areas in the insulation and the element's rigidity and damping. The connections between the surrounding walls and the sound propagation within the two rooms are also important, with the vibration eigenmodes of the excited rooms being a determining factor for the latter [1,2].

The airborne sound insulation provided has been studied for many years, with the first publications dating from the early part of the 20th century [3]. It was only in the middle of the last century, however, that London devised theoretical equations for calculating sound transmission via single and double walls [4–6], which stimulated research on simplified theoretical solutions for predicting the levels of acoustic insulation bestowed by building elements. Simplified methods have since been proposed to help design partition elements [7–11].

Research work has focused less on the low-frequency noise that commonly occurs in residential areas, even though today's world contains many outdoor sources of low frequency noise, which is less effectively reduced by walls and other protective structures [12–14].

Laboratory tests have been devised to determine the insulation provided by various elements, and the most commonly used technique is the two-room method [15–18]. However, the low-frequency range is not included in the standards for sound insulation measurements in use today. The sound reduction index for the low-frequency range has been shown to depend on parameters such as room size, sound source location and the reverberation time [12–14,19], making it hard to extrapolate test results to real-world situations, where rooms and separation elements alike vary greatly in terms of shape and size.

The reliability of the measurement of the acoustic insulation conferred by a dividing wall for sound frequencies lower than 100 Hz, for standard 50–70 m^3 European transmission rooms [20,21], is also open to question.

Osipov et al. [22] used three different models to predict low frequency airborne sound transmission through single partitions, namely, an infinite plate, a baffle plate and a room-plate-room. All these simplified models assume that the separating element is thin in comparison with the bending wavelength, and so Kirchhoff's harmonic pure bending wave motion theory is used. This method shows that acoustic insulation at low frequencies depends on the geometry and dimensions of the adjacent rooms, as well as on the properties of the wall.

The statistical energy analysis method (SEA) is one of the numerical schemes developed to predict the level of acoustic insulation provided by partition elements, and it has been usefully applied to complex problems of sound transmission [23–25]. An advantage of this method is that it uses statistical quantities, and so some details of the dynamic system are not needed. A drawback, however, is its lack of precision when the modal density is low.

Kropp et al. [26] developed a matrix formulation to calculate the acoustic insulation provided by a double element, at low frequencies, avoiding the problems caused by the thickness of the two panels of the wall, from which the Kirchhoff and Mindlin methods suffer. The same group also developed a model where the double element was composed of two flexible plates, joined together by an elastic layer and represented by uncoupled springs, not taking into account of shear stiffness.

Numerical techniques, such as the finite element (FEM) and finite difference methods, are seldom used to determine acoustic insulation because they require full discretization of the domain, with extremely fine meshes at high frequencies, which leads to a very high computational cost.

The FEM has been used, however, by Osipov et al. and by Maluski et al. [27,28] to analyse how a room's dimension influences the acoustic insulation provided by a partition at low frequencies. They also compared the numerical results with experimental findings, which revealed that sound insulation depends on the modal characteristics of the sound field in each room. Ljunggren [29] has recently verified, using theoretically simplified models, that the boundary and mounting conditions of single walls at low frequencies are expected to affect the sound reduction index.

Some of the methods described above simulate sound waves propagating through building partitions at low frequencies. Nearly all the methods described above, however, tend to assume only plane wave excitation and negligible fluid loading.

We have used the boundary element method (BEM) to compute the acoustic insulation provided by a single vertical panel, which separates two rooms when one of the rooms is excited by a steady-state, spatially sinusoidal, harmonic line load pressure at low frequencies. The limitations of thickness, referred to above, in the context of the Kirchhoff and Mindlin approaches, are avoided since the method adopted here fully models the rooms' surfaces and dividing wall, completely taking account of the coupling between the fluid (air) and solid structures. The present work focuses on the way the connection of the separating wall to the ceiling affects the acoustic insulation provided by the wall. Two distinct geometric models are analysed: first, where the wall is fixed to both the ceiling and floor; second, where the wall is fixed to the floor but there may be a gap between the wall and the ceiling (an acoustic barrier type structure). The second model is a more realistic model. It may be an acoustic screen, or it may be designed to allow cables and other equipment to pass between the wall and the ceiling.

The remainder of this paper is divided into four parts. First, the 3D problem is defined. Then, the BEM is formulated in the frequency domain and the results verified by applying them to a problem involving a cylindrical fluid-filled cavity, for which analytical solutions are known. Next, two distinct separating wall configurations, with different thicknesses and materials, are simulated, and the resulting sound pressure level difference between the two rooms, called acoustic insulation throughout this work, are compared. Finally, the computed results obtained with the acoustic barrier type structure are compared with those given by a rigid model.

2. BEM formulation

In the past decade, BEM models have emerged as very powerful tools for solving applied physics problems. One of the most important advantages of this method is that only the boundaries of the heterogeneities inside the domain being analyzed need to be discretized, rather than the domain itself. The BEM is particularly suitable for problems involving unbounded domains, because the Green's functions

used allow the far field radiation conditions to be satisfied. But the BEM leads to a fully populated system of equations, as opposed to the sparse system given by the finite difference and finite element techniques. Nevertheless, this technique is still efficient because the size of the system matrix is reduced.

The BEM has been used to simulate wave propagation between two fluid-filled boreholes, where the source and receivers are placed in different boreholes [30]. The technique thus reproduced is cross-hole surveying, a seismic prospecting technique that is often used to find the properties of an elastic medium separating two boreholes.

Bouchon [31] studied wave propagation in an infinite open borehole in layered isotropic media using the BEM, and his work was subsequently developed by Dong et al. [32], who refined the problem by adding casing to the borehole, and incorporating transversely isotropic layers. They used an indirect BEM to model the scattering from a source placed in both open and cased boreholes in transversely layered isotropic media.

Several authors have studied how geometric irregularities in a borehole affect acoustic response. Randall [33] and Tadeu et al. [30] simulated irregularities that might be caused by the mechanical action of the drill string in vertically inclined wells, or by rock collapse next to a borehole, plastic deformation, or washing a borehole drilled in soft or crumbling rocks, Bell et al. [34] and Zheng et al. [35].

The BEM model is employed in this work to calculate the three-dimensional pressure field generated by a steady-state, spatially sinusoidal, harmonic line load pressure inside two rooms separated by a wall or an acoustic barrier. A brief description of the BEM model is given below.

Fig. 1 represents the case where a concrete wall is used to separate two identical rooms. The floor, the ceiling and all the other walls of the rooms are also made of concrete, with density ρ, allowing a shear wave velocity of β and a compressional wave velocity of α. The fluid component (the air inside the rooms) has a density ρ_a and permits a compressional wave velocity α_a.

The geometric representation used does not model the outer boundaries of the floor, ceiling, and walls, that is, it assumes that the waves being transmitted to the slabs and exterior walls are not reflected back by the outer surface of these elements (see Fig. 1). Furthermore, it does not take into account the existence of walls placed along the z axis. So, the computed solution approaches that of two tunnels buried within an unbounded concrete medium. This procedure helps reduce the computational cost. These simplifications are nevertheless acceptable because the model described here is used to calculate the airborne sound insulation of the wall separating two rooms, and very little energy crosses the slabs and outer walls in comparison with what passes through the dividing wall.

One room contains a dilatational point source at position (x_0, y_0, z_0), and this oscillates with a frequency ω. The pressure incident field is expressed by

$$p_{\text{inc}} = \frac{A e^{i\frac{\omega}{\alpha_a}\left(\alpha t - \sqrt{(x-x_0)^2+(y-y_0)^2+(z-z_0)^2}\right)}}{\sqrt{(x-x_0)^2+(y-y_0)^2+(z-z_0)^2}} \tag{1}$$

where A is the wave amplitude and $i = \sqrt{-1}$.

The geometry of the rooms is assumed to be constant along the z direction, and so the 3D solution is arrived at by adding together a series of two-dimensional problems, for varying effective wavenumbers, $k_{\alpha_a} = \sqrt{(\omega/\alpha_a)^2 - k_z^2}$ with $\mathrm{Im} k_{\alpha_a} < 0$ [36], where k_z is the axial wavenumber once a Fourier transformation has been applied to the problem in the z direction. The incident field in this frequency wavenumber domain is given by

$$\hat{p}_{\mathrm{inc}}(\omega, x, y, k_z) = \frac{-iA}{2} H_0^{(2)}\left(k_{\alpha_a}\sqrt{(x - x_0)^2 + (y - y_0)^2}\right) \tag{2}$$

in which the $H_n^{(2)}(...)$ are second Hankel functions of order n.

As the rooms are modelled as though buried in unbounded medium, only the inner surfaces of the rooms have to be discretized, under the BEM. The BEM equations that are applied to this problem have already been applied by the authors to the solution of wave propagation in a fluid filled borehole [37]. The acoustic and

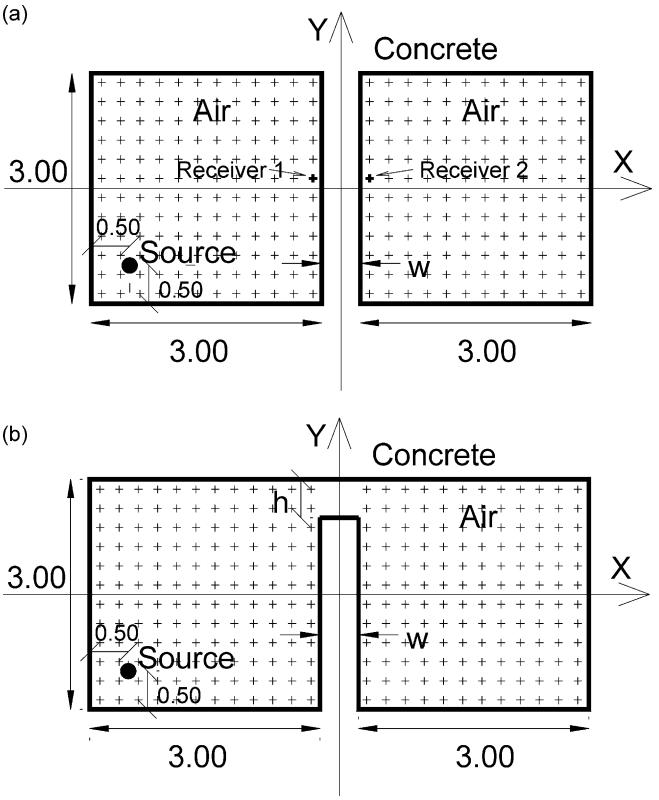

Fig. 1. Geometry of the problem (position of the sources and receivers): (a) Model 1—perfectly fixed connections between the wall and the floor, and between the wall and the ceiling; (b) Model 2—wall with a free end (wall/barrier).

elastic media are assumed to be homogeneous, and a perfect coupling between the solid and the fluid inside the rooms is held to exist. There is thus a continuity of normal displacements and stresses, and null tangential stresses at the interface between the solid and the fluid at the interface between the two media. A system of equations that can be solved for the nodal solid displacements and fluid pressures is devised by imposing these boundary conditions along the boundary of the fluid-filled rooms. This system of equations requires the evaluation of the following integrals along the appropriately discretized boundary of the rooms,

$$
\begin{aligned}
H_{ij}^{(s)kl} &= \int_{C_l} H_{ij}^{(s)}(x_k, x_l, n_l)\ dC_l \quad (i,j=1,2,3)\\
H_{a_1}^{(a)kl} &= \int_{C_l} H_{a_1}^{(a)}(x_k, x_l, n_l)\ dC_l\\
G_{ij}^{(s)kl} &= \int_{C_l} G_{ij}^{(s)}(x_k, x_l)\ dC_l \qquad (i=1,\ 2,\ 3;\ j=1)\\
G_{a_1}^{(a)kl} &= \int_{C_l} G_{a_1}^{(a)}(x_k, x_l)\ dC_l
\end{aligned}
\tag{3}
$$

in which $H_{ij}^{(s)}(x_k, x_l, n_l)$ and $G_{ij}^{(s)}(x_k, x_l)$ are the Green's tensor for traction and displacement components in the elastic medium, at point x_l in direction j caused by a concentrated load acting at the source point x_k in direction i; $H_{a_1}^{(a)}(x_k, x_l, n_l)$ are the components of the Green's tensor for pressure in the fluid medium, at point x_l caused by a pressure load acting at the source point x_k; $G_{a_1}^{(a)}(x_k, x_l)$ are the components of the Green's tensor for displacement in the fluid medium, at point x_l in the normal direction, caused by a pressure load acting at the source point x_k; n_l is the unit outward normal for the l^{th} boundary segment C_l; the subscripts $i, j = 1,\ 2,\ 3$ denote the normal, tangential and z directions, respectively. Standard vector transformation operators are used to transform these equations from the x, y, z Cartesian coordinate system. The Appendix gives details of the Green's functions and stress functions in Cartesian co-ordinates for the elastic and fluid media. The full derivation of these equations can be found at Tadeu et al. [38]. The integrations needed for Eq. (3) are carried out analytically for the loaded element [39,40], and when the element to be integrated is not the loaded element, a Gaussian quadrature scheme is used.

The internal material loss is considered using a complex Young's modulus and complex Lamé constants. The Young's modulus is computed as $E = E_r(1 + i\eta)$, where E_r corresponds to the classic modulus and η is the loss factor. The complex Lamé constants are written in the same form as the Young's modulus.

3. BEM validation

The validity of the BEM algorithm was verified by applying it to the solution of a circular cylindrical cavity driven in a concrete medium ($\alpha = 3499$ m/s, $\beta = 2245$ m/s

and $\rho = 2500$ kg/m^3), filled with fluid ($\alpha_a = 1500$ m/s and $\rho_a = 1000.0$ kg/m^3), when subjected to a dilatational harmonic pressure line load [with $A = 10{,}000$ in Eq. (1)], placed at point O (see Fig. 2), with $k_z = 1.0$ rad/m, for which the solution is known in closed form [41].

The response is calculated at two receivers placed inside (receiver 1) and outside (receiver 2) the fluid filled cavity. Computations are performed in the frequency range 1.0–800.0 Hz, with a frequency increment of 1.0 Hz. Fig. 3 displays the real and imaginary parts of the total pressure field and of the vertical displacements, calculated at receivers 1 and 2 respectively, when the inclusion is modeled with 30 boundary elements. The solid lines represent the analytical responses, while the marked points correspond to the BEM solution. The two solutions show very close agreement. Tests in which different loads and receivers were placed at different points gave equally good results.

4. Numerical applications

This section, describes the sound pressure level difference provided by a single vertical wall separating two identical rooms. Throughout this work, the sound pressure level difference conferred by the wall is termed acoustic insulation Two distinct geometries are used to model this separating wall: the first ascribes perfectly-fixed connections between the wall, the ceiling and the floor referred to Model 1 in this work (see Fig. 1a); the second model (Fig. 1b) is a fixed connection between the wall and the floor and a free connection on the other end to model the wall as a structural cantilever.

The rooms' floor, ceiling and wall surfaces are modelled with a number of boundary elements that increases with the frequency excitation of the dynamic source. The length of the elements is defined by the sound acoustic wavelength divided by 10. Given the small distance between the two faces of the separating wall, the length of boundary elements modelling the wall follows the above relation, but must also be at least 8 times less than its thickness. The same relation is applied to

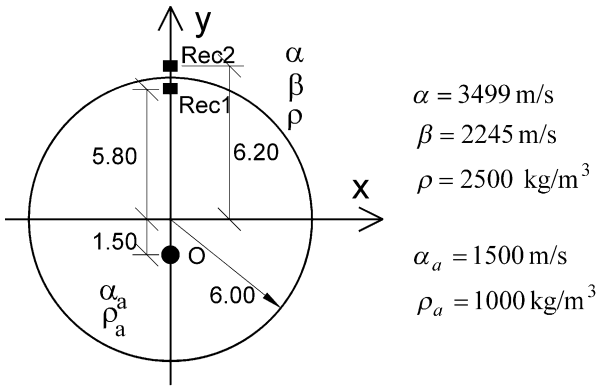

Fig. 2. Circular cylindrical fluid-filled cavity in an unbounded elastic medium.

the definition of the number of elements used to model the top edge of the wall in Model 2, with the distance between this edge and the ceiling being the reference distance.

The rooms are made from concrete, with the same properties as those used to validate the BEM model, and filled with air ($\alpha_a = 340$ m/s and $\rho_a = 1.22$ kg/m^3). The loss factor ascribed to the concrete is $\eta = 4 \times 10^{-3}$ [42]. The pressure wave field was computed along a grid of receivers placed in the two rooms, equally space, 0.25 m apart, along the vertical and horizontal directions, as illustrated in Fig. 1. A spatial harmonic line source placed in one of the rooms (source room) excites the full dynamic system (see Fig. 1). The calculations are performed for a frequency range from 1.0 to 800.0 Hz, with a frequency increment of 1.0 Hz. Some of the plots show the responses around specific frequency sub-domains, to better illustrate specific features of the computed results.

The computation of the response for a point pressure load would require a considerable computational effort, given the large number of 2D solutions that would have to be integrated. Simulations are thus performed following waves with different apparent wave velocities along the z-axis, to seek the main features of the 3D effects of a point source. This apparent wave velocity (c) is given by waves arriving at the z axis with a path inclination given by $arc\cos(\alpha_a/c)$, where α_a is the true wave velocity (see Fig. 4). Thus, in the equations presented above, k_z is taken to be ω/c.

Next, a cylindrical linear source ($k_z = 0$ rad/m) excites Model 1, where the separating wall is 0.10 m thick. This model is used to illustrate how the sound pressure level inside the two rooms is dependent on both the eigenfrequencies of the

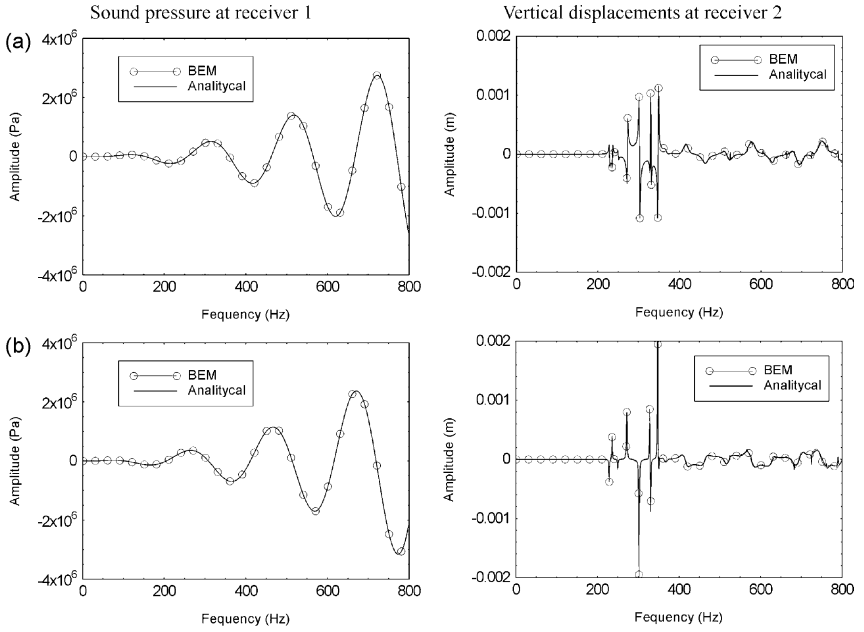

Fig. 3. Analytical versus BEM solution: (a) real part of the response; (b) imaginary part of the response.

rooms and on the transversal vibration modes of the wall. The average sound insulation, provided by the separating wall, is then computed for different wall thicknesses and for both models (Models 1 and 2). Model 2 has a gap of 0.05 m between the ceiling and the top edge of the separating wall. The displacements of the separating wall and the size of the gap are used to explain the average sound insulation differences between Models 1 and 2. The results for Model 2 are compared with those obtained assuming the existence of rigid walls and slabs. The importance of the rooms' surface conditions is assessed by modelling the rooms with cork. The average sound insulation provided by the two models is then obtained for a spatial sinusoidal harmonic source that generates waves, which propagate along the z direction with an apparent wave velocity of 400.0 m/s. Finally, a set of simulations is performed to study what effect a larger gap between the top of the wall and the ceiling has on the sound reduction provided by the dividing barrier.

4.1. Incidence of cylindrical waves of $k_z = 0$ rad/m

The different models were first subjected to the incidence of cylindrical linear waves of $k_z = 0$ rad/m, which corresponds to waves with an apparent wave velocity of $c = \infty$ m/s that are normally incident along the z direction. This corresponds to waves reaching the receivers with a 90° inclination in relation to the z axis (2D).

Fig. 5 gives the results when the source is placed on the first dynamic system defined by a separating wall, 0.10 m thick, perfectly fixed to the floor and ceiling (Model 1) in the frequency range sub domain from 1.0 to 200.0 Hz, to explain the main features of the response at very low frequencies more clearly. Fig. 5a displays the sound pressure level results, on a dB scale, obtained at the pair of receivers (1, 2), placed 0.125 m from the separating wall at 1.625 m from the floor, in the two rooms (see Fig. 1a). Receiver 1 is placed inside the source room, while receiver 2 is placed in the receiver room.

Stationary waves form and exercise a strong influence on the vibration properties of a room. These waves occur in the frequency domain according to the following equation [43,44],

$$f_{qr} = \frac{\alpha_a}{2}\sqrt{\left(\frac{q}{a}\right)^2 + \left(\frac{r}{b}\right)^2} \quad \text{(Hz)} \tag{4}$$

where a, b are the height and width of the room, and q and r are integers (0, 1, 2,....).

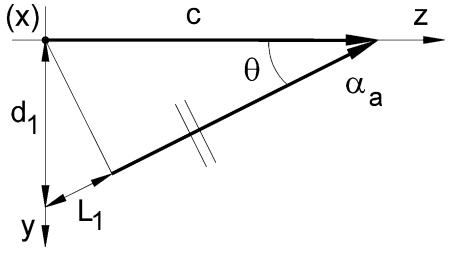

Fig. 4. Apparent wave velocity.

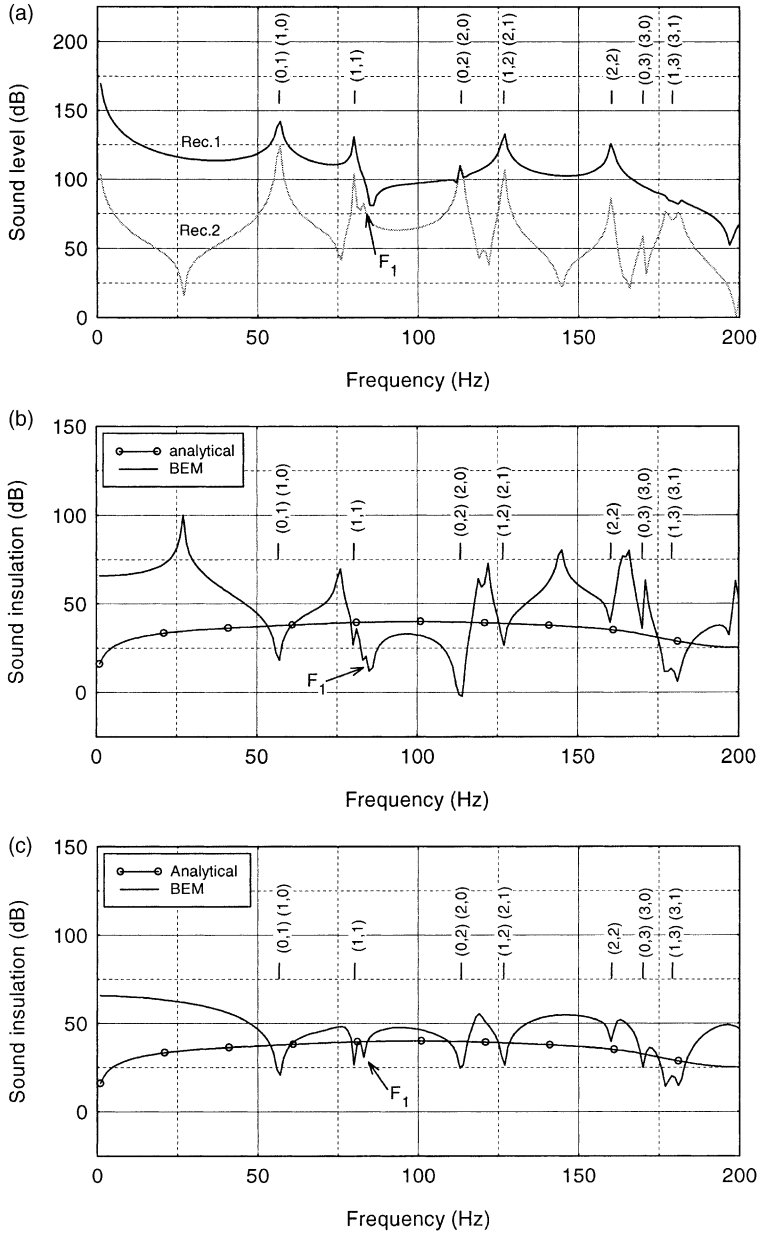

Fig. 5. Responses obtained when the source 2D ($k_z = 0$ rad/m) is excited in (Model 1) with a wall 0.10 m thick: (a) sound pressure level at receivers 1 and 2; (b) Sound insulation estimated by the receivers 1 and 2 versus the analytical solution for a wall of infinite extent; (c) Average sound insulation versus the analytical solution for a wall of infinite extent.

A dynamic source only excites modes, which do not exhibit null pressure at the position of the load. A fraction of the energy generated in the source room by the modes excited, passes through the separating wall to the receiver room. In the receiver room, this energy is seen as generated by an area source, which may excite additional modes. The dynamic process does not end here, since the energy in the receiver room is also transmitted to the source room, where it can be observed as a weak area source, exciting additional modes. The results in Fig. 5a corroborate this interpretation: at receiver 1, the sound pressure level field exhibits enhanced peaks in the vicinity of the first excited modes [$f_{10} = f_{01} = 56.67$ Hz, $f_{11} = 80.14$ Hz, $f_{02} = f_{20} = 113.33$ Hz, $f_{12} = f_{21} = 126.71$ Hz and $f_{22} = 160.28$ Hz]. The modes [$f_{03} = f_{30} = 170.0$ Hz and $f_{13} = f_{31} = 179.2$ Hz] are not excited in the source room since the pressure load is placed over a nodal line of these stationary modes (0.5 m away from the neighbouring boundaries of the source room). These are clearly seen in the sound pressure level responses registered in the second room, which correspond to the excitation of these modes; small peaks in the neighbourhood of these later modes occur in the responses for the first room, caused by energy being transmitted from the second room to the first.

Other dips of sound insulation are still visible in the vicinity of specific frequencies not associated with the normal modes of the rooms. These dips are generated by the vibration of the wall, and change according to its thickness. The response confirmed that this first peak appears in the vicinity of the first eigenmode of the structural system, labeled F_1 in Fig. 5 ($f = 83.0$ Hz). To better illustrate this phenomenon, Fig. 6 displays the real part of the displacement of the mid plane of the wall, which exhibits symmetric behavior in relation to its mid height.

Fig. 5b displays the sound insulation estimated by receivers 1 and 2. As expected, low insulation is registered in the vicinity of the eigenmodes of the room. Fig. 5b also includes the response obtained when the wall is infinite and bounded by air media on both faces. These solutions were previously obtained analytically, taking into account the air-solid interaction, and can be found in Tadeu et al. [45,46].

Analysis of this figure shows that the computed sound pressure level difference between the registered sound pressure level at the receivers 1 and 2 indicates pronounced dips and troughs not predicted by the analytical model. The discrepancies between the results obtained by the two models, are particularly important at very low frequencies, where the BEM solution predicts higher insulation results than those anticipated by the analytical model.

The contribution of the coincidence effect [47], which is associated with propagation of waves along the wall, in the results provided by Model 1, is not well-defined. The analytical solution obtained for a wall of infinite extent agrees with this interpretation. It can be seen that the dip related to the coincidence effect is not sharp, but appears as a smooth change in the frequency domain at around 200 Hz. Its contribution to the response thus confirms that there is not a pronounced dip associated with the coincidence effect.

Notice, that the coincidence effect phenomenon results from the movement of the wall panel caused when it is struck by inclined sound waves with a wavelength that equals that of the wall bending waves. When the contribution of the air to the

movement of the wall is not considered, the frequency associated with the coincidence effect is given by

$$\omega = \left(\frac{\alpha_a}{\sin\phi}\right)^2 \sqrt{\frac{\rho h}{D}} \tag{6}$$

where ϕ is the angle of incidence of the sound, h is the thickness of the panel, $\omega = 2\pi f$, $D = \left(h^3 E\right)/\left[12\left(1-\nu^2\right)\right]$, E is the Young's modulus (N/m2), ν is Poisson's ratio and ρ is the density of the panel's material (kg/m3). The critical frequency corresponds to the case when ϕ is equal to 90°, which leads to a value of 185.1 Hz. The analytical model that takes the coupling between the air and the solid into account predicts higher values.

Fig. 5c displays the average sound insulation calculated from the response computed over a grid of 144 receivers, equally spaced 0.25 m apart along the vertical and the horizontal directions, placed in each room (see Fig. 1). The resulting curve is smoother than the pressure level difference calculated between receivers 1 and 2, and approaches the results given by the analytical model, particularly for frequencies above 50 Hz. However, the computed response is still highly dependent on the excited modes of the rooms, revealing poor insulation in the vicinity of the corresponding eigenfrequencies. As for receivers 1 and 2, the analytical model predicts insulation lower than that computed by the BEM model at very low excitation frequencies.

Fig. 7 displays the averaged sound insulation provided by a separating wall 0.10 or 0.20 m thick inserted in Models 1 and 2. The average values have been computed along the same grid of 144 receivers placed in each room. Fig. 7a shows the results obtained by Model 1. The features of the responses do not appear to change significantly as the thickness of the wall changes. The insulation dips still occur in the vicinity of the eigenmodes of the dynamic system. As expected, the highest average sound insulation is obtained when the wall is 0.20 m thick. However, the results do

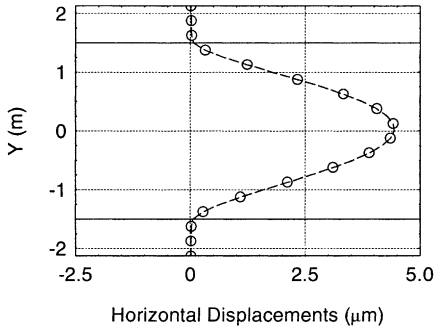

Fig. 6. Horizontal displacements of the mid plane of a vertical wall, 0.10 m thick, inserted in Model 1,

not show a constant increase in sound insulation as we move from a wall 0.10 m thick to a wall 0.20 m thick, oscillating markedly throughout the frequency domain. Notice that the analytical model responses included in this figure follow the trend of the insulation variation registered by Model 1.

Fig. 7b presents the results obtained for Model 2, where the separating wall/barrier is loosely connected to the ceiling, with a gap of 0.05 m between the ceiling and the top of the wall. Dips of sound insulation for walls 0.10 and 0.20 m thick still occur in the vicinity of the eigenmodes of the rooms. Frequency shifts in the position of the eigenmodes of the rooms are found when we move from Model 1 to Model 2. As before, additional dips in sound insulation are still found in the vicinity of specific frequencies associated with the vibration of the wall (the first modes are labelled F_2 in the plots). The sound insulation provided by the 0.20 m thick wall is still better than that given by the wall 0.10 m thick. However, the increase in sound insulation is small compared with that in Model 1 when doubling thickness.

Comparing the results of Models 1 and 2 (Figs. 7a and b), Model 2 clearly gives a much lower average sound insulation than Model 1, particularly at very low frequencies. The results thus indicate that the wall-ceiling gap plays an important role in the sound insulation provided by the separating wall.

To better understand the contribution of the movement of the separating wall on the definition of sound insulation, an additional simulation was performed with a BEM model that assumes the existence of rigid wall boundaries. The BEM code has been previously used by the authors to define the acoustic scattering of a three-dimensional sound pressure source by an infinitely long rigid barrier in the vicinity of a tall building [48]. Fig. 7c plots the insulation curves provided by the two models when the separating wall is 0.20 m thick. Analysis of the results confirms that the responses are similar except in the vicinity of the frequencies associated with the eigenmodes related to the movement of the elastic separating wall. This again explains that the drop of sound insulation from Model 1 to Model 2 is mainly due to the sound travelling through the gap. As mentioned above, the sound insulation provided by the 0.20 m thick wall/barrier is slightly better that that provided by the wall/barrier 0.10 m thick. This behaviour is only explained by the differences in the horizontal length of the gap.

The horizontal displacements of the dividing wall have been calculated to help understand the sound transmission mechanisms through the separating wall. Fig. 8 shows the real part of the computed horizontal mid-plane wall displacements for both models and for the two wall thicknesses. The results for excitation frequencies of 10.0 and 150.0 Hz, are displayed. The horizontal wall displacements of Model 2 exhibit much larger displacements than those of the Model 1, which means that far more energy passes through the separating wall/barrier. It can also be observed that the horizontal wall displacements of the thinner wall/barrier, in the case of the Model 2, are not always greater than those for the thicker wall/barrier (see Fig. 8b). This behaviour again shows that the difference in sound insulation that is given by a wall/barrier 0.10 m thick from that by one that is 0.20 m thick is mainly due to the passage of the sound waves through the gap between the wall and ceiling.

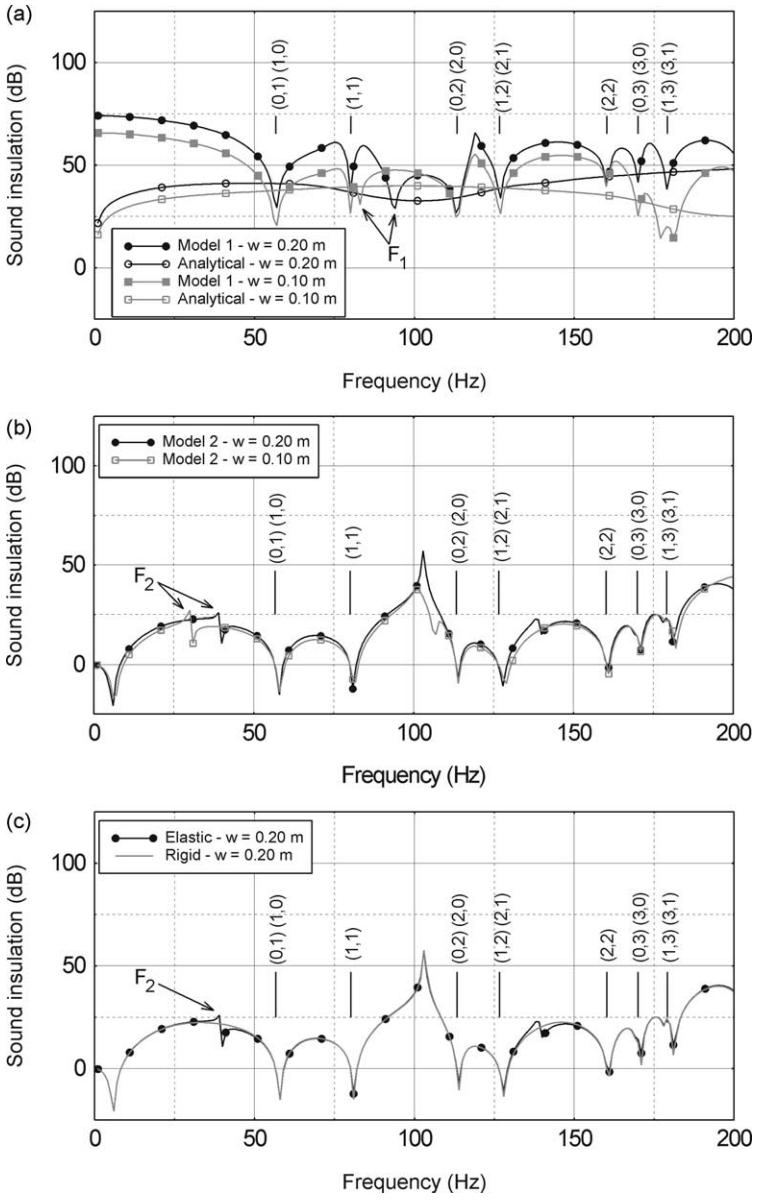

Fig. 7. Average sound insulation ($k_z = 0$ rad/m): (a) elastic BEM response of walls 0.10 m and 0.20 m thick inserted in Model 1 versus the analytical solution for an infinite extent walls; (b) Elastic BEM response of walls 0.10 and 0.20 m thick inserted in Model 2 (air gap of 0.05 m); (c) Rigid versus elastic BEM response of a wall 0.20 m thick inserted in Model 2 (air gap of 0.05 m).

The largest average sound insulation difference given by the results from Models 1 and 2, occurs in the vicinity of the eigenmodes associated with the vibration of the separating wall. Fig. 9 displays the real part of the calculated horizontal wall displacements, for both models, in the vicinity of the first vibration eigenmode of the wall in Model 2, when the wall is 0.10 and 0.20 m thick. As expected, much larger displacements are registered for the wall in Model 2 than in Model 1, which contribute to the big sound insulation difference between Models 1 and 2 in the vicinity of these frequencies.

An additional simulation has been performed to assess the importance of the rooms' surface conditions, where concrete is replaced by cork ($\alpha = 431$ m/s, $\beta = 283$ m/s, $\rho = 140$ kg/m^3 and $\eta = 0.15$ [42]). Fig. 10 presents the sound insulation of the 0.20 m wall placed in Models 1 and 2 (0.05 m gap). The results show that the dips related to the modal behaviour of the rooms are not as sharp as those displayed before. This behaviour is explained by the amount of energy that is now transmitted through the boundaries of the rooms, given that cork is not as rigid as concrete. The drop in sound insulation between Model 1 and Model 2 is not as

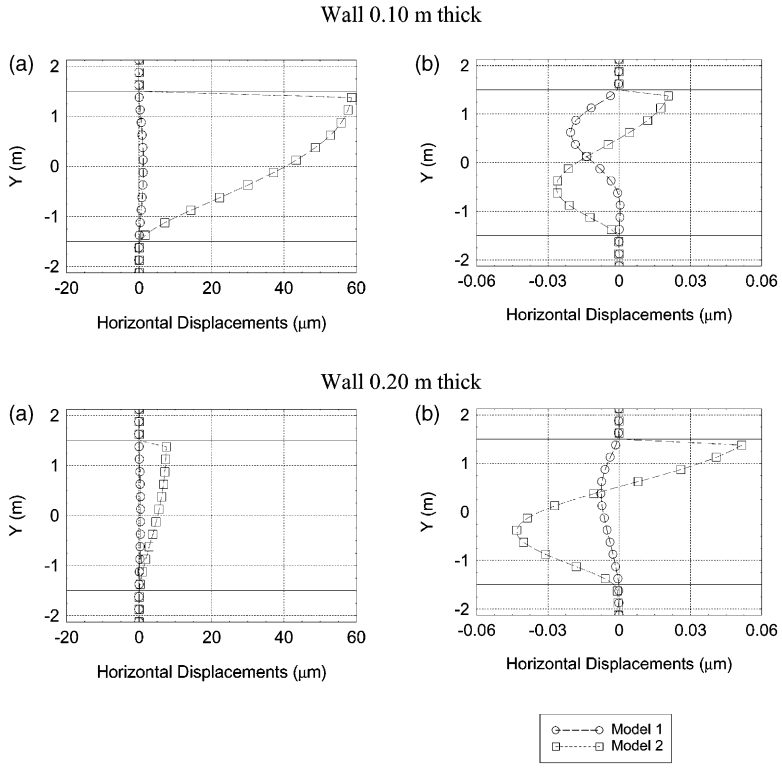

Fig. 8. Horizontal displacements of the mid plane of separating walls, 0.10 and 0.20 m thick, inserted in Models 1 and 2 (air gap of 0.05 m) generated by a 2D source ($k_z = 0$ rad/m): (a) 10.0 Hz; (b) 150.0 Hz.

pronounced as before. Fig. 10 also includes the sound insulation predicted by the analytical model, which suggests that it is closer to the results given by Model 1.

4.2. Incidence of cylindrical waves of $k_z \neq 0$ rad/m

A wall 0.20 m thick is used to illustrate how the acoustic insulation changes when a wall panel is subjected to the incidence of cylindrical waves with different spatial sinusoidal variation along the axis of the room. In the example given, an apparent velocity of $c = 400.0$ m/s is chosen. This apparent wave velocity corresponds to waves reaching the surface of the rooms with an inclination of 58.2° in relation to the z direction of the surface.

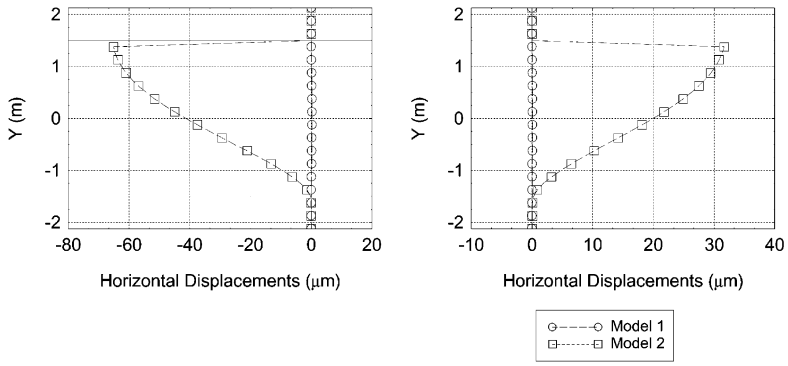

Fig. 9. Horizontal displacements of the mid plane of separating walls inserted in Models 1 and 2 (air gap of 0.05 m) when subject to a 2D source ($k_z = 0$ rad/m): (a) wall 0.10 m thick at 31.0 Hz; (b) wall 0.20 m thick at 40.0 Hz.

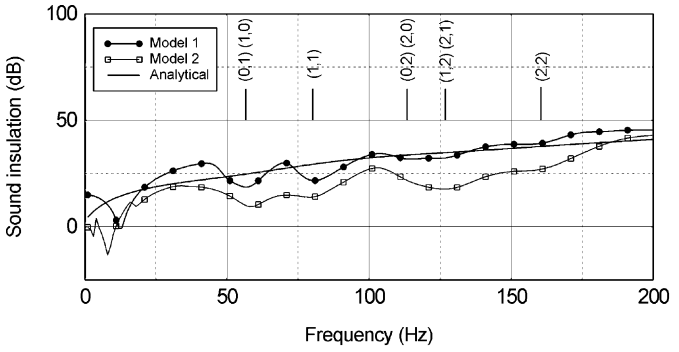

Fig. 10. Responses obtained when the source 2D ($k_z = 0$ rad/m) is excited in Models 1 and 2 (air gap of 0.05 m) with a wall 0.20 m thick, when the material properties of cork have been attributed to the boundaries of the rooms. The analytical solution for a wall of infinite extent is also included.

Fig. 11 displays the response of the two models. The main features of the results are the same as those described above. When the wall is perfectly connected to the ceiling (Model 1), the dips in the sound pressure insulation occur at very well defined frequency positions, which coincide with the eigenmodes of a room with dimensions $3.0\sin(31.8) = 1.58$ m [$f_{10} = f_{10} = 107.57$ Hz and $f_{11} = 152.13$ Hz]. This happens because the travel distance (L_1) in this domain is smaller, since it corresponds to the projection of the initial vertical path (d_1) on the inclined path, leading to a distance $L_1 = d_1\sin[arccos(\alpha_a/c)]$ (see Fig. 4).

As before, particularly at low frequencies, Model 2 predicts lower sound insulation than Model 1. It can also be seen that dips of insulation associated with the eigenmodes of the room in Model 2 occur in the vicinity of the eigenmodes of the rooms in Model 1, but with a small frequency shift. The comparison of the present results with those provided when the source is two-dimensional ($k_z = 0$ rad/m) shows that the insulation provided by the walls is greater when $k_z \neq 0$ rad/m in the presence of Model 1.

4.3. Sound insulation provided by an acoustic barrier separating two rooms

Using Model 2, the importance of the gap between the ceiling and the wall is investigated by increasing the original gap to 0.20 m. The new model is named Model 2′. The average sound insulation computed for the three models when the separating wall is 0.10 m thick and the source is excited in the frequency range from 1.0 to 800.0 Hz, is now given. Fig. 12 displays the computed BEM results when the source emits cylindrical waves with an apparent wave velocity of $c = \infty$ m/s.

The acoustic insulation is generally lower than that predicted by the other models, particularly at low frequencies. However, the insulation computed still exhibits dips and peaks that are associated with the vibration eigenmodes of the two rooms. The comparison of the results for the three different models shows that there is a big drop in sound insulation when the connection of the wall to the ceiling is no longer fixed, that is, when we move from Models 1 to 2. Once the connection between the

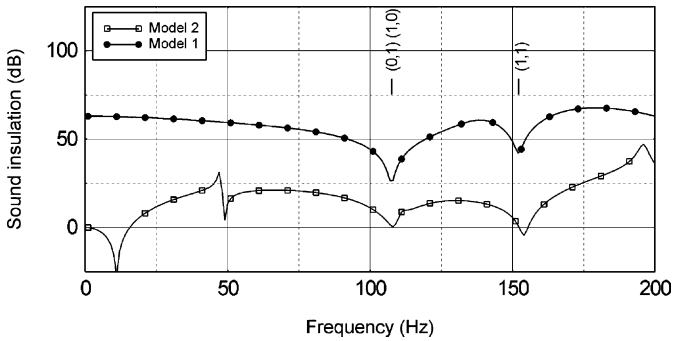

Fig. 11. Average sound insulation when the source, with a spatial sinusoidal variation along the z of $c = 400.0$ m/s, is excited in Models 1 and 2 with a separating wall 0.20 m thick.

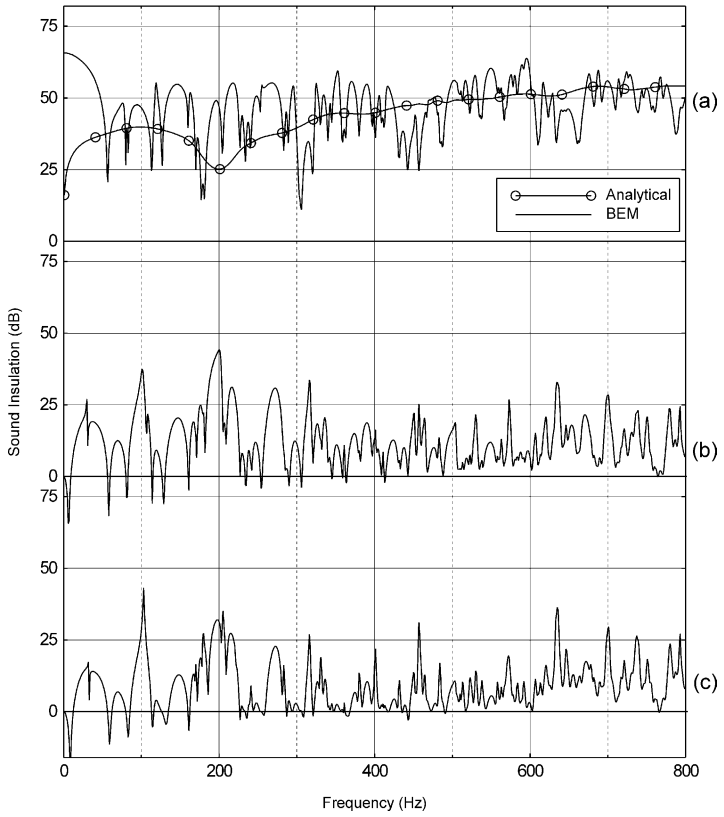

Fig. 12. Average sound insulation when a 2D source ($k_z = 0$ rad/m), is excited in the presence of a separating wall 0.10 m thick: (a) Elastic BEM response when the wall is inserted in Model 1 versus the analytical solution for a wall of infinite extent; (b) Elastic BEM response when the wall is inserted in Model 2 with an air gap of 0.05 m; (c) elastic BEM response when the wall is inserted in Model 2′ with an air gap of 0.20 m.

wall and the ceiling is loose, the size of the gap between the top of the separating wall and the ceiling appears to have a relatively much smaller effect on the fall in sound insulation.

Several simulations were performed for different wall thicknesses and for sources emitting cylindrical waves with other apparent wave velocities. The results are not plotted here, since the sound insulation features are similar to the ones above described.

5. Conclusions

The boundary element method was formulated in earlier work [37] and implemented to calculate the sound insulation provided by a wall separating two rooms,

at low frequencies. The model fully considers the dynamic coupling between the fluid (air) and the solid walls and does not limit the thickness of the wall, as Kirchhoff and Mindlin theories need to do.

Once validated, the model was used to define how the connection of a wall to the ceiling affects the acoustic insulation provided by the wall. Two different wall configurations, double-fixed, and barrier-type structure, were simulated. The responses were computed for low frequency sources generating cylindrical waves with spatial sinusoidal variation along the z direction.

The computed results show that the sound insulation provided by a wall is highly dependent on the vibration modes excited in the rooms, and on the way the separating wall is connected to the ceiling. A loose connection causes a substantial drop in the acoustic insulation provided by the wall. This fall in acoustic insulation is largely explained by the energy that travels through the gap between the barrier and the ceiling. The improvement in acoustic insulation when the wall is thicker is much smaller for a wall with a free end than for a wall with a fixed end to both floor and ceiling.

It should be noted that in real-life situations other variables would contribute to the definition of the sound insulation provided by a separating wall or barrier: for example, a wall along a third dimension would create a more complicated modal behaviour of the rooms; a thickness restriction for the slabs and the walls would create additional scattering phenomena that would reintroduce more energy to the rooms, and additional dips from reflections associated with the modal response of the structure. Even though these extra factors may occur, features similar to those envisaged by the present model could also be expected to be present.

Appendix A. The Green's functions

A.1. Solid formation

Definitions:

λ, μ		Lamé constants
ρ		Mass density
$\alpha = \sqrt{(\lambda + 2\mu)/\rho}$		P wave velocity
$\beta = \sqrt{\mu/\rho}$		S wave velocity
$k_p = \omega/\alpha$	$k_s = \omega/\beta$	
$k_\alpha = \sqrt{k_p^2 - k_z^2}$	$k_\beta = \sqrt{k_s^2 - k_z^2}$	
$A = \dfrac{1}{4i\rho\omega^2}$		Amplitude
$\gamma_i = \dfrac{\partial r}{\partial x_i} = \dfrac{x_i}{r}\ i = 1,\ \ 2$		Direction cosines

$H_{n\alpha} = H_n^{(2)}(k_\alpha r)\ H_{n\beta} = H_n^{(2)}\left(k_\beta r\right)$ Hankel functions

$B_n = k_\beta^n H_{n\beta} - k_\alpha^n H_{n\alpha}$ B_n functions

Green's functions for displacements

$$G_{xx} = A\left[k_s^2 H_{0\beta} - \frac{1}{r}B_1 + \gamma_x^2 B_2\right]$$

$$G_{yy} = A\left[k_s^2 H_{0\beta} - \frac{1}{r}B_1 + \gamma_y^2 B_2\right]$$

$$G_{zz} = A\left[k_s^2 H_{0\beta} - k_z^2 B_0\right]$$

$$G_{xy} = G_{yx} = \gamma_x \gamma_y A B_2$$

$$G_{xz} = G_{zx} = ik_z \gamma_x A B_1$$

$$G_{yz} = G_{zy} = ik_z \gamma_y A B_1 \tag{A.1}$$

Volumetric strain (super-index = direction of load)

$$\begin{aligned}\varepsilon_{\mathrm{Vol}}^l &= G_{xl,x} + G_{yl,y} + G_{zl,z} \\ &= A\left[\frac{\partial}{\partial x_l}\left(k_s^2 H_{0\beta}\right) + B_{0,xlx} + B_{0,yly} + B_{0,zlz}\right] \\ &= A\frac{\partial}{\partial x_l}\left[k_s^2 H_{0\beta} + B_{0,xx} + B_{0,yy} + B_{0,zz}\right] \\ &= A\frac{\partial}{\partial x_l}\left[k_s^2 H_{0\beta} + \hat{\nabla}^2 B_0\right]\end{aligned} \tag{A.2}$$

Note: $H_{0\beta,l} = -k_\beta \gamma_l H_{l\beta} \quad H_{0\beta,z} = -ik_z H_{0\beta}$

Strain components (tensor definition, not engineering)

$$\begin{aligned}\varepsilon_{ij}^l &= \frac{1}{2}\left(G_{il,j} + G_{jl,i}\right) \\ &= \frac{1}{2}A\left(\delta_{il}k_s^2 H_{0\beta,j} + \delta_{jl}k_s^2 H_{0\beta,i} + B_{0,ilj} + B_{0,jli}\right) \\ &= \frac{1}{2}k_s^2 A\left(\delta_{il}H_{0\beta,j} + \delta_{jl}H_{0\beta,i}\right) + AB_{0,ijl}\end{aligned} \tag{A.3}$$

(a) Strains for loads in the plane, $l = x, y$

$$\varepsilon^l_{\mathrm{Vol}} = \gamma_l A\left(-k_s^2 k_\beta H_{1\beta} + k_z^2 B_1 + \frac{4}{r}B_2 - B_3\right)$$
$$\varepsilon^l_{xx} = \gamma_l A\left(\left(\frac{2}{r}B_2 - k_s^2 k_\beta H_{1\beta}\right)\delta_{xl} + \frac{1}{r}B_2 - \gamma_x^2 B_3\right)$$
$$\varepsilon^l_{yy} = \gamma_l A\left(\left(\frac{2}{r}B_2 - k_s^2 k_\beta H_{1\beta}\right)\delta_{yl} + \frac{1}{r}B_2 - \gamma_y^2 B_3\right)$$
$$\varepsilon^l_{zz} = \gamma_l k_z^2 A B_1$$
$$\varepsilon^l_{xy} = A\left(\left(\frac{1}{r}B_2 - \frac{1}{2}k_s^2 k_\beta H_{1\beta}\right)\left(\delta_{xl}\gamma_y + \delta_{yl}\gamma_x\right) - \gamma_x\gamma_y\gamma_l B_3\right)$$
$$\varepsilon^l_{xz} = ik_z A\left(\left(\frac{1}{r}B_1 - \frac{1}{2}k_s^2 H_{0\beta}\right)\delta_{xl} - \gamma_x\gamma_l B_2\right)$$
$$\varepsilon^l_{yz} = ik_z A\left(\left(\frac{1}{r}B_1 - \frac{1}{2}k_s^2 H_{0\beta}\right)\delta_{yl} - \gamma_y\gamma_l B_2\right) \tag{A.4}$$

(b) Strain for axial loads, $l = z$

$$\varepsilon^z_{\mathrm{Vol}} = ik_z A\left(-k_s^2 H_{0\beta} + k_z^2 B_0 + \frac{2}{r}B_1 - B_2\right)$$
$$\varepsilon^z_{xx} = ik_z A\left(\frac{1}{r}B_1 - \gamma_x^2 B_2\right)$$
$$\varepsilon^z_{yy} = ik_z A\left(\frac{1}{r}B_1 - \gamma_y^2 B_2\right)$$
$$\varepsilon^z_{zz} = ik_z A\left(-k_s^2 H_{0\beta} + k_z^2 B_0\right)$$
$$\varepsilon^z_{xy} = -ik_z\gamma_x\gamma_y A B_2$$
$$\varepsilon^z_{xz} = \gamma_x A\left(-\frac{1}{2}k_s^2 k_\beta H_{1\beta} + k_z^2 B_1\right)$$
$$\varepsilon^z_{yz} = \gamma_y A\left(-\frac{1}{2}k_s^2 k_\beta H_{1\beta} + k_z^2 B_1\right) \tag{A.5}$$

(c) Stresses

$$\tau^l_{ij} = \lambda\varepsilon^l_{\mathrm{Vol}}\delta_{ij} + 2\mu\varepsilon^l_{ij} \tag{A.6}$$

A.2. Fluid formation

Definitions:

λ_a	Lamé constant
ρ_a	Mass density
α_a	P wave velocity
$k_{pa} = \omega/\alpha_a$	
$k_{\alpha a} = \sqrt{k_{pa}^2 - k_z^2}$	
$A_a = \frac{1}{4i}$	Amplitude
$\gamma_i = \frac{\partial r}{\partial x_i} = \frac{x_i}{r}\ i = 1,\ 2$	Direction cosines
$H_{n\alpha a} = H_n^{(2)}(k_{\alpha a} r)$	Hankel functions

Green's functions for displacements

$$\begin{aligned} G_{ax} &= -A_a k_{\alpha a} H_{1\alpha a} \gamma_x \\ G_{ay} &= -A_a k_{\alpha a} H_{1\alpha a} \gamma_y \end{aligned} \tag{A.7}$$

Stresses

$$H_{a1} = A_a \lambda_a H_{0\alpha a}\left(-\omega^2/\alpha_a^2\right) \tag{A.8}$$

References

[1] Beranek LL, Vér IL. Noise and vibration control engineering, principles and applications. New York: Wiley; 1992.

[2] Tadeu A, Mateus D. Sound transmission through single, double and triple glazing. Experimental evaluation. Applied Acoustics 2001;62(3):307–25.

[3] Lord Rayleigh. The theory of sound. New York: Dover; 1945.

[4] London A. Transmission of reverberant sound trough double walls. J Acoustical Soc of Am 1950;44: 270–8.

[5] London A. Transmission of reverberant sound trough single walls. J Research Nat Bur of Stand 1949;42:605.

[6] London A. Transmission of reverberant sound trough double walls. J Research Nat Bur of Stand 1949;44:605.

[7] Cremer L. Theorie der Shalldämmung dünner Wände bei schrägem Einfall. Akust Z 1942;7:81–102.

[8] Sewell EC. Transmission of reverberant sound through a single-leaf partition surrounded by an infinite rigid baffle. Journal of Sound and Vibration 1970;12:21–32.

[9] Sharp BH. Prediction methods for the sound transmission of building elements. Noise Control Engineering 1978;11:53–63.

[10] Callister JR, George AR, Freeman GE. An empirical scheme to predict the sound transmission loss of single-thickness panels. Journal of Sound and Vibration 1999;222(1):145–51.

[11] Novikov II. Low-frequency sound insulation of thin plates. Applied Acoustics 1998;54(1):83–90.

[12] Mathys J. Low frequency noise and acoustical standards. Applied Acoustics 1993;40(3):185–200.

[13] Berglund B, Hassmen P, Soames RF. Sources and effects of low-frequency noise. Journal of the Acoustical Society of America 1996;99(5):2985–3002.

[14] Kropp W, Pietrzyk A, Kihlman T. On the meaning of the sound reduction index at low frequencies. Acta Acustica 1994;2:379–92.
[15] International Standardization Organization—ISO 140-3. Acoustics, measurement of sound insulation in buildings and of building elements, laboratory measurements of airborne sound insulation of building elements. 1978.
[16] International Standardization Organization—ISO 140-10, Acoustics, measurement of sound insulation in buildings and of building elements, measurement of sound insulation of small building elements. 1989.
[17] American Society for Testing and Materials—ASTM E90, Standard test method for laboratory measurement of airborne sound transmission loss of building partitions. 1990.
[18] International Standardization Organization—ISO 140-1, Acoustics, measurement of sound insulation in buildings and of building elements, requirements for laboratories. 1990.
[19] Gagliardini L, Roland J, Guyader JL. The use of a functional basis to calculate acoustic transmission between rooms. Journal of Sound and Vibration 1991;145(3):457–78.
[20] Roland J, Villenave M, Gagliardini L, Soubrier D. Contract no. 3165/1/0/078/87/7-BCR-B(30) CSTB. Intercomparation of measurements of noise attenuation by double glazed windows in frames. 1991.
[21] Pedersen DB, Roland J, Raabe G, Maysenholder W. Measurement of the low-frequency sound insulation of building components. Acustica- acta acustica 2000;86(3):495–505.
[22] Osipov A, Mees P, Vermeir G. Low frequency airborne sound transmission through single partitions in buildings. Applied Acoustics 1997;52(3/4):273–88.
[23] Craik RJM. Sound transmission through buildings using statistical energy analysis. Hampshire, England: Gower Publishing Limited; 1996.
[24] Hynnä P, Klinge P, Vuoksinen J. Prediction of structure-borne sound transmission in large welded ship structures using statistical energy analysis. Journal of Sound and Vibration 1995;180(4):583–607.
[25] Craik RJM, Smith RS. Sound transmission through double leaf lightweight partitions part I: airborne sound. Applied Acoustics 2000;61:223–45.
[26] Kropp W, Rebillard E. On the air-borne sound insulation of double wall constructions. Acústica-acta acústica 1999;85:707–20.
[27] Osipov A, Mees P, Vermeir G. Numerical simulation of airborne sound transmission at low frequencies: the influence of the room and the partition parameter. Proceedings of Inter-Noise 1997;97: 2 759–762.
[28] Maluski SPS, Gibbs BM. Application of a finite-element to low-frequency sound insulation in dwellings. J Acoust Soc Am 2000;108(4):1741–51.
[29] Ljunggren L. Airborne sound insulation of single walls at low frequencies: a discussion on the influence of boundary and mounting conditions. Building Acoustics 2001;8(4):257–67.
[30] Tadeu A, Santos P. 3D Wave propagation in fluid-filled irregular boreholes in elastic formations. Journal of Soil Dynamics and Earthquake Engineering 2001;21(6):499–517.
[31] Bouchon M. A numerical simulation of the acoustic and elastic wavefields radiated by a source in a fluid-filled borehole embedded in a layered medium. Geophysics 1993;58:475–81.
[32] Dong W, Bouchon M, Toksöz MN. Borehole seismic-source radiation in layered isotropic and anisotropic media: boundary element modeling. Geophysics 1995;60:735–47.
[33] Randall CT. Modes of noncircular fluid-filled boreholes in elastic formation. J Acoust Soc Am 1991; 89:1002–16.
[34] Bell JS, Gough DI. Northeast-southwest compressive stress in Alberta—evidence from oil wells. Earth Planet Sci Lett 1979;45:475–82.
[35] Zheng Z, Kemeny K, Cook NGW. Analysis of borehole breakouts. J Geophy Res 1989;94:7171–82.
[36] Bouchon M, Aki K. Discrete wave-number representation of seismic source wavefields. Bull Seism Soc Am 1977;67:259–77.
[37] Tadeu A, Godinho L, Santos P. Wave motion between two fluid filled boreholes in an elastic medium. EABE- Engineering Analysis with Boundary Elements 2002;26(2):101–17.
[38] Tadeu A, Kausel E. Green's functions for two-and-a-half dimensional elastodynamic problems. Journal of Engineering Mechanics, ASCE 2000;126(10):1093–7.
[39] Tadeu A, Santos P, Kausel E. Closed-form integration of singular terms for constant, linear and

quadratic boundary elements—Part I: SH wave propagation. EABE- Engineering Analysis with Boundary Elements 1999;23(8):671–81.
[40] Tadeu A, Santos P, Kausel E. Closed-form integration of singular terms for constant, linear and quadratic boundary elements—Part II: SV-P wave propagation. EABE- Engineering Analysis with Boundary Elements 1999;23(9):757–68.
[41] Pao YH, Mow CC. Diffraction of elastic waves and dynamic stress concentrations. Rand Corporation, 1973.
[42] Cremer L, Heckl M, Ungar EE. Structure-borne sound. Berlin: Sringer-Verlag; 1988.
[43] Kuttruff H. Sound in enclosures. Encyclopedia of acoustics—vol. 3, Wiley; 1997.
[44] Kang SW, Lee JM, Kang YJ. Vibration analysis of arbitrarily shaped membranes using non-dimensional dynamic influence function. Journal of Sound and Vibration 1999;221(1):117–32.
[45] Tadeu A, António J. 2.5D Green's functions for elastodynamic problems in layered acoustic and elastic formations. J Computer Modeling in Eng and Sciences 2001;2(4):477–95.
[46] Tadeu A, António J. Acoustic insulation of single panel walls provided by analytical expressions versus the mass law. Journal of Sound and Vibration [in press].
[47] Beranek LL. Noise reduction. New York: McGraw-Hill; 1960.
[48] Godinho L, António J, Tadeu A. 3D sound scattering by rigid barriers in the vicinity of tall buildings. Journal of Applied Acoustics 2001;62(11):1229–48.